Flipping the sign of refractive index changes in ultrafast and temporally shaped laser-irradiated borosilicate crown optical glass at high repetition rates

A. Mermillod-Blondin,[1] I. M. Burakov,[2] Yu. P. Meshcheryakov,[3] N. M. Bulgakova,[2] E. Audouard,[1] A. Rosenfeld,[4] A. Husakou,[4] I. V. Hertel,[4,*] and R. Stoian[1,†]

[1]*Laboratoire Hubert Curien, UMR 5516 CNRS, Université Jean Monnet, 42000 Saint Etienne, France*

[2]*Institute of Thermophysics SB RAS, 630090 Novosibirsk, Russia*

[3]*Design and Technology Branch of Lavrentyev Institute of Hydrodynamics SB RAS, 630090 Novosibirsk, Russia*

[4]*Max-Born-Institut für Nichtlineare Optik und Kurzzeitspektroskopie, 12489 Berlin, Germany*

(Received 14 December 2007; revised manuscript received 18 February 2008; published 26 March 2008)

Ultrafast subpicosecond laser exposure usually induces negative refractive index changes in optical glasses with strong thermal expansion such as borosilicate BK7 due to volume expansion and mechanical rarefaction. We show that temporally shaped laser excitation on picosecond scales and at high repetition rates can invert the regular material response resulting in a significant refractive index increase. Simulations of pulse propagation and evolution of heat and strain waves in BK7 glass exposed to different pulse durations were performed to understand mechanisms of refractive index increase. Narrow spatial distribution of energy for optimized picosecond pulses determines shock-induced plastic deformations accompanied by partial healing of the lateral strain due to preferential heat flow. The matter momentum relaxation produces directional on-axis material compaction.

DOI: 10.1103/PhysRevB.77.104205 PACS number(s): 61.80.Ba, 42.65.−k, 65.40.De, 81.40.Tv

I. INTRODUCTION

Achieving control on matter transformations by energetic beams has beneficial consequences for material processing applications. Irradiation creates physicochemical material changes, building up on deviations from charge, thermal, or mechanical equilibrium. Fast energy deposition is able to induce unique structural material phases due to extreme pressure and temperature regimes generated inside the material.[1,2] Concerning application fields, consequences have emerged for three-dimensional structuring of materials. Due to the particularly strong energy localization, ultrafast laser radiation was successfully employed for generating photonic structures in glasses suitable for optical integration.[3] Specifically, ultrashort pulse lasers were employed in waveguide writing techniques. This is due to positive refractive index variations that result from structural rearrangements of the dielectric matrix.[4–8] The sudden nonlinear electronic excitation triggers a sequence of transformations defined by the spatiotemporal character of excitation and by the material response. Local material modification may be induced in the form of color centers or reordering of chemical bonds caused by electronic and thermal effects.[9–12] Using laser techniques, waveguiding objects were created in fused silica (a-SiO_2), which is one of the commonly used optical materials. Here the excited material quenches in a densified form involving a change in the bonding angle.[10] However, for multicomponent or more complex glass structures, the laser action is more difficult to be deciphered.[4,5] Local atomic displacements concur with macroscale phenomena in a complex way to generating a refractive index change. Generally, the response to optical excitation depends on the relaxation properties of the glass and the extrapolation of the waveguide writing technique to other materials may not be able to demonstrate the same degree of success as for a-SiO_2. In many borosilicate and phosphate glasses with high expansion coefficients, ultrafast laser action results in a dominant negative refractive index change due to volume expansion. The guiding region is restricted to stressed material around the exposed low density region,[13,14] being detrimental for symmetric mode guiding. In these conditions, the possibility to reverse this natural tendency toward rarefaction into a compaction regime carries both technological and fundamental significances.

Having in mind refractive index modifications and their potential in optical technologies, we address here the issue of material transformation under regulated energy feedthrough. We explore the effects of laser-induced plasticity in establishing a desired type of refractive index redistribution. The purpose is identifying, activating, and understanding laser-induced mechanisms for material compaction. Using temporal pulse shaping and a comprehensive theoretical analysis involving nonlinear optical energy deposition, thermodynamic evolution, and mechanical relaxation, we demonstrate that the hydrodynamic flow of softened material can be guided to form an extended region of compressed matter. This leads, under specific conditions of laser energy delivery, to a positive refractive index change, which is an inversion of the regular material response.

We concentrate on a model glass with dominant "thermal" character, which is defined as such from relaxation considerations.[14] A representative, BK7, a borosilicate crown glass, is a low cost material with applications in optics and microfluidics. It is characterized by slow electronic relaxation, high thermal expansion, and low softening point. These properties are characteristic to a large class of glassy materials. BK7 usually shows a decrease of the refractive index under ultrafast laser exposure.[4,5] The reason is associated with the formation of a hot region, where, due to rapid thermal expansion, the material is quenched in a low-density phase rich in oxygen centers.[5] Understanding that this conduct, apart from the chemical aspect, depends on the heating and relaxation rates, we explore the conditions to reverse it

using adaptive temporal pulse shaping.[15] This study indicates ways of controlling matter response to energetic beam excitation. The formation of positive refractive index or the flexibility in creating local dielectric optical properties has consequences for the design of light-guiding devices.

From the experimental point of view, several strategies were put forward for waveguide writing. Low repetition rates (kilohertz) were often used, building up on the effect of individual pulses.[13,16] High repetition rates (megahertz) were more recently involved, taking advantage on thermal cumulative effects.[17–19] The intermediate region (100 kHz) was equally explored for generating waveguiding structures in several materials.[3,4,20] We concentrate our discussion on this regime, which corresponds to the time scale of mechanical relaxation and discuss the role of macroscopic stress in generating spatial patterns of refractive index variations, in addition to potential changes at atomic level.[12] While static mechanical effects are always present, contributing among other factors to glass densification, acting on the mechanical relaxation time scale may induce particular stress patterns. Stress actions may be used in writing guiding structures in complex materials.[21] The 100 kHz pulse repetition rate is then particularly interesting since it provides the prerequisites (in terms of temporal window) of controlling both heat and stress actions[12] during multipulse exposure.

The paper is organized as follows. The experimental sections provide an overview of the irradiation setup and the adaptive loop, together with a demonstration of index flipping. The modeling section gives insights into the simulation tools, coupling together nonlinear pulse propagation and thermomechanical material response. Section IV concentrates the discussion on several issues. First it describes qualitatively the aspect of laser-induced structures in view of possible nonlinearities and the follow-up relaxation. It shows how a pulse temporal form may trigger a transition from negative to positive index variation, which gradually extends under rapid multipulse excitation. The role of stress relaxation and heat dynamics in relation to material compaction is indicated, in particular, irradiation conditions involving picosecond pulses. This, in turn, allows waveguide writing in optimal conditions. A possible thermomechanical scenario is discussed.

II. EXPERIMENTAL SECTION

A. Experimental setup

BK7 parallelepipedic samples were irradiated with 150 fs pulses from an 800 nm Ti:sapphire ultrafast laser system at a rate of 100 kHz. The exposure time was controlled by an electromechanical shutter. The laser beam was focused inside at a depth of 200 μm by a microscope objective (numerical aperture, 0.45) to a waist of approximately 0.9 μm. At this depth, optical aberrations play a negligible role.[22] In this regime of relatively tight focusing, linear and nonlinear propagation effects are equally observable, allowing a good exploitation of the temporal features of the pulse.

Detection of the relaxed structures is realized in real time by Zernike-type positive optical phase-contrast microscopy (PCM). A charge-coupled device camera delivers a side image of the spatially resolved relative changes in the refractive index induced by irradiation. The phase-based microscopy arrangement allows detection from a submicrometer thick layer located at the center of the structure. It thus provides a qualitative picture of the refractive index change. Positive or negative optical phase changes relative to the background can be evaluated based on the image gray-value shift. Correspondingly, dark regions denote positive index changes, while the light zones indicate a negative refractive index variation or the presence of light scattering centers.

The laser system incorporates a programmable liquid-crystal pulse-shaping apparatus, which realizes temporal pulse tailoring using spectral phase filtering.[15] This device has the role to disperse, manipulate, and recollimate the spectral frequency components of the pulse, allowing for spectral phase modulation and subsequent pulse temporal design. A feedback loop connects the microscopy detection and the pulse control unit, being guided by an adaptive optimization algorithm (evolutionary strategy).[23] The pulse tailoring unit performs the variation of the incoming temporal intensity and the detection of the refractive index delivers the quantitative evaluation of the laser action. The laser pulse envelope is iteratively changed with the purpose of generating a desired index pattern. The loop involves recording the two-dimensional (2D) map of the photoinscribed phase object and the comparison to a designer target profile. The evaluation is made along a median line, which sections axially (along the laser direction) the detected phase map. An axial index profile is thus obtained. The target mask is defined by an extended axial region of positive index change with a high contrast. In our case, a target profile with a Gaussian form was used and compared with the laser-induced axial index profile, as will be described in the following section. The accuracy of the profiles is defined by the microscope resolution. The adaptation of the detected axial profile to the target profile defines the success of the irradiation sequence. A set of arbitrary phase patterns is initially applied on the optical modulator and evolves through genetic propagators. Results are ranked according to the degree of similarity between the detected phase object and the desired target. Next, the algorithm suggests an improved collection of excitation envelopes. The solution space is thus explored iteratively in an evolutionary manner.[24] The optimization result is an intensity shape that has produced index patterns close to the desired target. Having noticed that ultrafast laser irradiation produced a negative index change in BK7, we have applied the adaptive loop to create a dominant region of positive refractive index variation.

B. Optimization results

We review below the results of irradiation at 100 kHz pulse repetition rate. Figures 1(a) and 1(b) show the static laser multipulse modification traces for two experimental conditions: short pulse (SP) (150 fs) and optimal pulse (OP). The OP is the laser pulse provided by the adaptive loop when attempting to maximize positive refractive index changes according to a user profile target. Irradiation dose corresponds to 5×10^4 laser pulses at 0.17 μJ per pulse. The SP morphol-

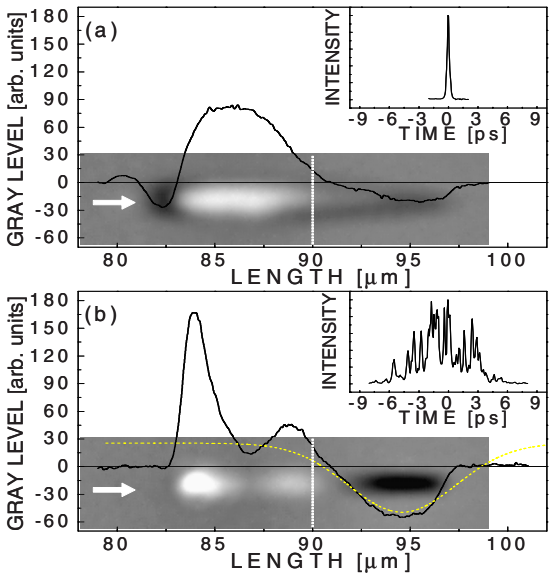

FIG. 1. (Color online) (a) PCM observation of the accumulated effect of 5×10^4 short pulses in BK7 at 150 fs, 0.17 μJ, and 100 kHz and the corresponding axial gray-level cross section. White color indicates a negative index change or, in certain cases, the presence of light scattering centers. The laser pulse is incident from the left. The best focus is located at $z=90$ μm. The inset shows the incident pulse temporal shape. (b) Observation of the cumulative effect of 5×10^4 optimal pulses in BK7 irradiated by the same energy as in (a) and the corresponding axial cross section. The black color corresponds to a positive index change. The target profile is also represented (dotted line). The inset shows the incident pulse temporal shape.

ogy is defined by a negative index change region extending all over the irradiated zone. This region appears white in the PCM image, with a strip of positive index material surrounding laterally the modified region. The OP trace shows the onset of a significant black region at the tip of the trace, corresponding to a positive refractive index change. The final profile shows a good match to the target mask (dotted line in Fig. 1) in the relevant region of positive index change. Nevertheless, despite the compaction effect, a wide white region remains, suggesting a tradeoff in mass redistribution.

The arguments explaining the optimal pulse result on the material are extracted from a dual analysis: temporal characterization of the optimal pulse and simulation of the excitation traces. The OP temporal profile [inset in Fig. 1(b)] shows a noisy but recognizable picosecond envelope. Apparently, in spite of the presence of femtosecond spikes, the material follows the behavior induced by a picosecond pulse since the slower electronic relaxation convolutes all the fast actions into a slower varying temporal envelope. The result was confirmed using chirped pulses generated by the spatial light modulator. Results of multipulse irradiation at 100 kHz repetition rate and at various pulse durations are given in Fig. 2. A transition between a region of dominant negative index change and positive index variation is noted around 1 ps. This suggests the apparition of physical circumstances able to trigger factors of material compaction. It will be shown in the next sections that these circumstances are related to the

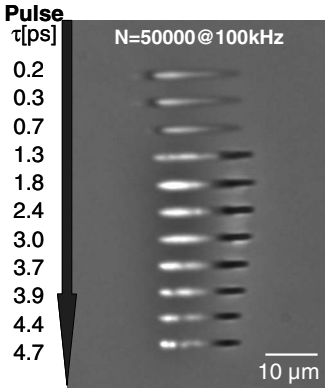

FIG. 2. PCM observation of the accumulated effect of 5×10^4 laser pulses in BK7 at 0.17 μJ, 100 kHz, and different pulse durations. The black and white colors correspond, respectively, to a positive refractive index change and to an index decrease.

picosecond envelope and to the high repetition rate. No influence of the chirp sign is noted, suggesting that the pulse envelope is the driving factor rather than the frequency distribution in the pulse.

It is worth noticing here that picosecond results are not uncommon for quality structuring of bulk glasses. Due to the stronger localization of energy, they show in several occasions benefits with respect to femtosecond irradiation and they were successfully applied in three-dimensional glass processing or interface melting.[25,26]

III. SIMULATION APPROACH

Once the generating pulse profiles were determined, a fundamental issue relates to the spatial aspect of the excited region in different irradiation conditions. The interaction involves a complex sequence of processes, from nonlinear energy deposition to relaxation toward a final structural configuration. As a first step, we performed simulations of a Gaussian pulse propagation inside the transparent material by solving the nonlinear Schrödinger equation.[27,28] The purpose is to identify the characteristics of femtosecond and picosecond excitation behaviors. The solution takes into account key features of photoionization, plasma defocusing, and self-focusing, as detailed in Ref. 28. Further effects include diffraction, multiphoton and avalanche ionization, group-velocity dispersion, space-time coupling, and energy losses on the free electrons. The parameters are the same as in Ref. 28, except for characteristic material properties (group velocity dispersion $k''=446$ fs^2/cm, nonlinear refractive index $n_2=3.45\times10^{-16}$ cm^2/W, energy gap $E_{g0}=4.2$ eV, and reduced effective mass $m=m_e$). The damping factor of the electron plasma was chosen to be $\omega_0\tau_c=3$, implying electronic dephasing on the femtosecond scale. The electron density is described by a rate equation, which takes into account three-photon ionization accompanied by collisional multiplication.[27] We have used an experimentally determined three-photon absorption coefficient $\sigma=7\times10^{17}$ cm^{-3} ps^{-1} (cm^2/TW)^3 for borosilicate glasses.[29,30]

The numerical solution that describes laser excitation allows insights into several dominant processes. First we men-

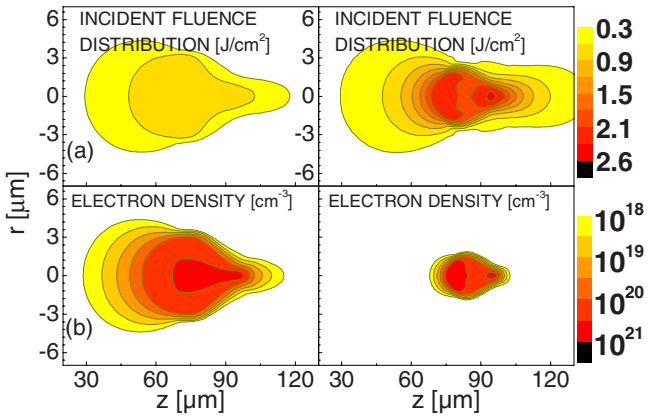

FIG. 3. (Color online) (a) Incident fluence and (b) electron density distributions at the end of the laser pulse in the case of a single short pulse (left) and a 4.5 ps long pulse (right) in BK7 at 0.5 μJ. The focal point is at $z=90$ μm.

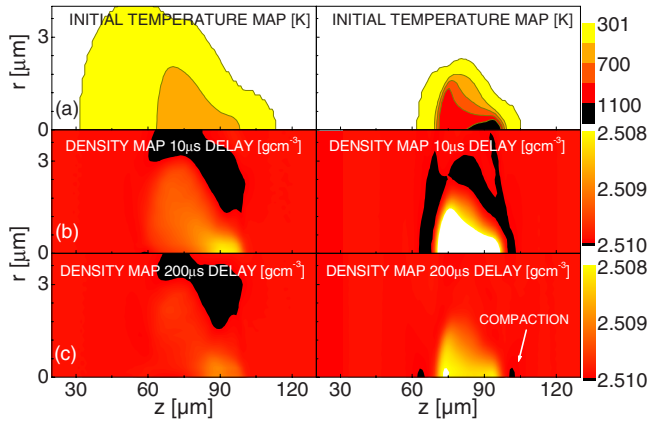

FIG. 4. (Color online) (a) 2D-contour maps of the absorbed energy (given as the temperature increase in the glass matrix) in the case of a single short pulse (left) and a 4.5 ps long pulse (right) in BK7 at 0.5 μJ. The focal point is at $z=90$ μm. (b) The subsequent material density map obtained after numerically cooling the exposed area for 10 μs. The black regions correspond to compressed material. (c) Density map obtained after a significantly longer time (200 μs).

tion that the average power threshold corresponding to a visible modification under the present experimental conditions corresponds approximately to 5 mW (0.06 μJ). This low value rests roughly six times below the critical power for self-focusing (for BK7 the critical peak power is 1.96 MW, corresponding to 30 mW of average power). A main consequence emerges. Under tighter focusing conditions, efficient generation of plasma occurs in the early stages of the pulse, well before the activation of the self-focusing mechanisms. Insights into the incident irradiation features and the subsequently generated electron plasma density in case of a single 150 fs short pulse and a 4.5 ps long pulse in BK7 are given in Fig. 3. Two main qualitative differences may be noted between the short and the long pulse regimes. The axial size of the irradiated zones is not the same. The reason is related to the plasma formation and its dynamics in the two cases. Strong ionization in the prefocal region ($z \leqslant 90$ μm) for the femtosecond pulse causes significant energy defocusing by the emerging plasma. Scattering of the light pulse redistributes laser energy on a wider region around the focal zone. If in both cases (femtosecond and picosecond) the plasma density stays subcritical, it has a slightly higher peak for the picosecond case. The plasma density peak is delayed in the picosecond case toward the end of the pulse. Self-focusing also depletes the focal region energetically due to an axial back spreading of energy, an effect which is more important for the femtosecond pulse.

However, the most important quantity in our case is related to energy absorption. This reflects the spatial redistribution of energy removed from the laser pulse by multiphoton and bremsstrahlung absorption. This quantity, once relaxed to the glass matrix, determines the spatial characteristic of the modification trace as the region where the energy concentration stays above a certain threshold. Figure 4(a) shows the absorbed energy distribution as temperature achieved in the glass matrix for single pulse exposure using short (left) and long (right) pulses. The total absorption rate is 60% in the SP case. The OP shows an overall lower absorption rate of 35%. As mentioned above, the laser-induced electronic plasma attains significant densities later in the laser pulse and causes less light defocusing. The energy feedthrough is not obturated and the maximum absorbed energy density is higher for the picosecond case, forming a narrow structure with a strong z-axis temperature gradient. The energy is allowed to concentrate in the focal region leading to higher temperatures. In the narrow axial region, the softening point is surpassed. The maximum temperature (1600 K) is approximately 2.5 times higher than the femtosecond counterpart but less than the decomposition temperature of 2000 K.

As a second step of the simulation, the absorbed energy maps were connected to a dynamic thermal elastoplastic Lagrangian model for deformations inside laser-irradiated glasses. The absorbed energy (ρ_E), which is equivalent to an instantaneous temperature field, evolves in time according to the material thermomechanic properties. This assumption is justified as long as the energy transfer to the glass matrix occurs on a picosecond scale, much shorter than the mechanical response. Due to the fast relaxation, the material follows a quasi-isochoric path to the hot state, which subsequently cools by diffusion. The temperature rise is calculated as $\Delta T=\rho_E/(\rho c)$, where $\rho \simeq 2.5$ g/cm^3 is the material density and $c=0.878$ J/g K is the specific heat. In calculating the induced stress,[31] the approach based on the finite element method combines standard equations of dynamic elasticity (equation of motion and Hook's law) with the von Mises yield criterion for plastic yielding[32] and allows us to model structural deformations of the heated material. Stress tensor components are calculated assuming cylindrical symmetry. A detailed presentation of the model and its assumptions can be found in Ref. 33. We mention that the model takes into account phenomena such as heat transfer, dynamic elasticity, and material deformations with plastic yielding. It iteratively follows the changes in temperature and the subsequent variations in the stress and density fields in the assumption that glass viscosity is large enough and cooling takes place with-

out strong elastic waves. In view of the complexity of the approach and the present knowledge of material parameters, the model gives a qualitative indication of material behavior trends under laser excitation.

IV. RESULTS AND DISCUSSION

Based on the simulations, the following sequential scenario emerges for the specified exposure energy domain. The laser pulse creates a hot pressurized region. The initial pressures are 0.2 GPa for the SP and 0.7 GPa for the OP. Thermal expansion commences and, in the first nanoseconds, an elastoplastic wave (EPW) is launched.[34] The amplitude of the EPW depends on the initial temperature increase and on the material mechanical properties, notably on the expansion coefficient. The compression wave propagates away from the hottest zone, generating plastic deformation as an extended envelope around a rarefied core.[35,36] The main factor is a particularly strong thermal expansion coefficient, which is approximately 15 times higher than for a-SiO_2, in the conditions where a-SiO_2 has a higher mechanical resistance and an elevated softening point. As the compressed shell is formed, the plastic zone is defined by the tangential stress reaching the yield value (7 MPa). Outside of the plastified shell, the material is in an elastically compressed state and hoop stress develops. The heat wave follows on a microsecond scale. Due to the elongated shape of the heat source, elastoplastic and heat waves dissipate faster on axis as compared to the radial direction. The last stage is the relaxation of the elastically compressed outer region upon cooling followed by mass redistribution. The positive value of the hoop stress favors inward relaxation. If this is a common scenario for both femtosecond and picosecond pulses, we will focus below on specific differences able to trigger different thermomechanical behaviors.

We recall that the femtosecond induced heat source has a large size and the temperature is below the softening point. A quasicylindrical geometry of heat diffusion occurs. We have verified the state of the distorted matter at 10 μs [Fig. 4(b), left], which corresponds to the temporal distance between two consecutive laser pulses and as well on a longer time of 200 μs [Fig. 4(c), left], which is representative for a permanent modification. The dense regions formed by the EPW 3 μm away from the axis stay below the softening temperature and cool down in several microseconds without further density change. A steady state appears, with no material motion occurring between 10 and 200 μs. The nonrelaxed plastic shell acts as a barrier preventing backward extension of the elastically compressed outer region. In this time, the hoop stress relaxes from 1 to 0.8 MPa. Subsequent pulses will preserve the lateral deformation due to repeated EPWs, which are too weak to induce axial densification.

Concerning the picosecond sequence, the density maps after cooling indicate that the axial extension of the compressed zone occurs [Figs. 4(b) and 4(c), right]. A dense region appears closer to the core due to the EPW advance and remains until the arrival of the heat wave. Since the picosecond heat source is narrower with a significantly higher temperature, it favors a stronger radial heat wave. When the thermal wave reaches the lateral periphery (less than 1 μs), the densified envelope softens. At this moment, the hoop stress in the elastic region amounts to a value of 12 MPa. Stress release occurs from the elastic region, removing the deformation. The passing of the heat wave provides an unloading factor toward the central rarefied region. The release of the lateral plastified shell allows the inward expansion of the outer elastically compressed region. The hoop stress decays further from a value of 3 MPa at 10 μs to 2 MPa at 200 μs creating a compressional effort toward the axis. As seen in Figs. 4(b) and 4(c), at 10 μs, the material has not yet reached the steady state. The hoop stress is stronger in the radial directions of the plastically compressed zone as compared to the axial zones so its release occurs nearly cylindrical. This determines the partial healing of the periphery parts of the plastic shell due to material redistribution toward the structure axis. The core of the structure is still fairly hot, counteracting to the radial material flow and thus redirecting it axially. Thus, during the central action of the hoop stress, matter is pressed out sidewise and redistribution in the axial direction occurs. This is assisted by the conical aspect of the structure. The larger sized prefocal region [Fig. 4(a)] cools slower. The high temperature is preserved longer, providing a conical pressure profile. Material is shifted to the conoid tip, gaining a preferential axial direction of densification at the borders of the focal region. Agglomeration follows a matter momentum gain supported by the back action of the outer elastic region. Matter undergoes quasidirectional flow and moves away from a dynamics governed mainly by thermal expansion. As a summary of the above discussion, a schematic overview of the processes taking place in the case of picosecond irradiation is given in Figs. 5(a)–5(c), showing the formation of the plastic shell due to the EPW, the subsequent softening due to the heat wave, and the release of stress from the elastically compressed region with density redistribution. It has to be noted that, as compared to femtosecond pulses, picosecond pulses couple energy more efficiently only above a certain input threshold, which corresponds to an appreciable electronic density. In the vicinity of the observable modification threshold, the ultrashort pulses excite the material more efficiently. This topic is currently under investigation.

The simulations are performed for single pulses (which explain the higher energy compared to the experiment) and deviations from the experimental results should be expected. The compression effect induced axially by a single pulse is dimensionally small with respect to the rarefaction zone. The relative density axial increase is also reduced, being approximately 10^{-4}. However, for this processing window, indications on material behavior can be extracted. The question then refers to the relevance of the single pulse higher energy simulation as compared to multipulse excitation at lower energies. Even though the incubation effects are reduced for BK7 especially at low repetition rates,[37] they nevertheless exist and their understanding requires detailed investigations on the microscale. Their effect intensifies for picosecond pulses due to a reduced nonlinearity of absorption. The consequence is that the absorption cross section increases under multipulse excitation, gradually providing a better coupling for the picosecond pulses, so that higher energy results may

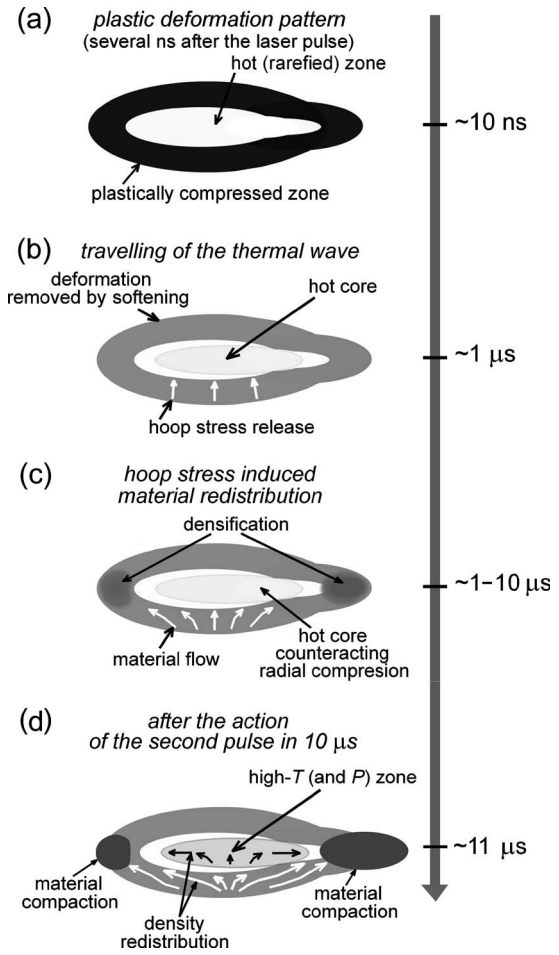

FIG. 5. Qualitative description of thermomechanical processes induced by picosecond laser irradiation. The picture emphasizes matter redistribution stages for single pulse irradiation: (a) the formation of the plastic layer as a result of the EPW, (b) softening of the plastic region upon heating, and (c) stress release and density redistribution. (d) The potential effect of a subsequent pulse arriving on approximately 10 μs is represented as well.

become relevant. Returning to the simulation results, some of the consequences are readily recognizable: axial compression and lateral stress release due to strong heat wave. Based on the higher energy results, the qualitative view can partly be extended to a multipulse sequence under optimal conditions. Already after the first pulse, the residual temperature at 10 μs shows an excess of 70 K. This implies that, for the present heat source sizes, there may be a slow and gradual temperature increase with the number of pulses[17] which may further assist in lateral stress healing. Also, as was already mentioned, the lateral hoop stress has an enhanced value before the arrival of the next pulse and it is also slowly accumulated with the number of pulses, creating a stronger effort toward the material compaction for pulses arriving on the microsecond time scale. This constitutes an additional mechanical memory of excitation, which is a familiar phenomenon in excited dielectrics.[37] A qualitative indication of this process is given in Fig. 5(d). When a subsequent picosecond pulse arrives at 10 μs time delay and generates a new elastoplastic wave, the latter produces a new plastic shell on

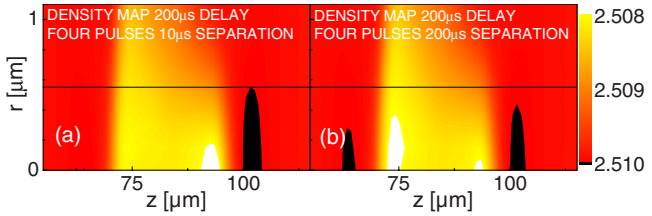

FIG. 6. (Color online) Multipulse structures (N=4) induced at different repetition rates: 100 kHz (left) and 5 kHz (right) for 0.5 μJ picosecond pulses. The density map is observed at 200 μs after the last pulse in the sequence. The index increase rate per pulse is higher in the high repetition rate case as compared to the low repetition rate regime.

the background of the previous structure remains and the process is repeated. In approximately 1 μs after this second pulse, the thermal wave covers the plastic shell and the latter is softened. The released hoop stress pushes the material toward the axis but the counteraction of the hot zone leads to the considerable on-axis compaction of the material at the structure tip. Due to a conical geometry of the structure, matter is shifted preferentially in the direction of the laser pulse propagation. Compaction of the material takes place on a wider on-axis zone as compared to the initial structure. When subsequent pulses arrive, the thermal waves generated by them do not cover completely the on-axis compaction zones and they cause further on-axis agglomeration of the material. The material is compressed with each heating cycle in the direction of the laser pulse, creating extended on-axis region of pressurized material. This was verified with calculations for double, triple, and quadruple pulse exposures at high repetition rates where a gradual density increase of few percent per pulse was observed, with a higher rate as compared to the low repetition rate case. An example is depicted in Fig. 6 for a sequence of four pulses. At low repetition rates, the single and the multipulse structures are remarkably similar, showing the low significance of long-living incubative effects. Experimentally as well, the increase of the compaction zone was noted after several hundreds of pulses at a

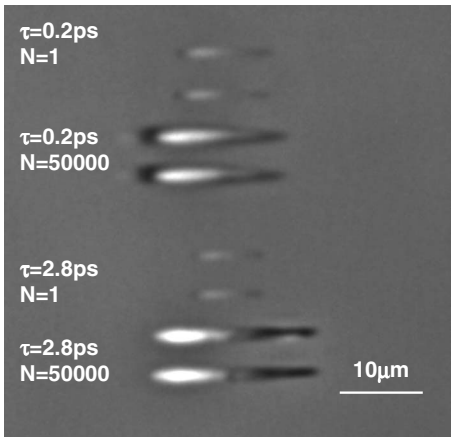

FIG. 7. Comparison between single and multipulse regimes at different pulse durations and 0.2 μJ input energy. The compaction is becoming significant in the picosecond multipulse regime.

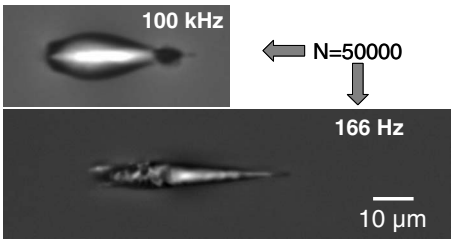

FIG. 8. High energy multipulse structures (1.1 μJ) induced in BK7 by 150 fs pulses at different laser repetition rates (see text for details). A compacted region surrounding a low density core is visible for the 100 kHz structures (top). The lower repetition rate structure has a more damaged appearance (bottom).

high repetition rate. The difference between the single pulse and multipulse regime is marked in Fig. 7, showing the visible axial densification at the tip of the picosecond multipulse sequence.

It should be noted that if instructive indications are gathered with respect to the tendency of material behavior, not all the observed features are fully explained. The model should be further corroborated with changes on the microscopic scales.

The refractive index flip has consequences for waveguiding applications. The translation of the SP index profile (negative index change) is unlikely to produce a waveguide in the absence of a hydrodynamic motion that compresses material on axis. Increasing the SP energy may achieve a certain axial compression. This is depicted in Fig. 8, which gives the high energy (1.1 μJ) multipulse irradiation result in BK7 for 150 fs laser pulses at different repetition rates. A compression shell surrounding a rarefied core appears for the high energy 100 kHz structure, which prolongates on the axis. The 166 Hz structure has a more damaged appearance that deviates from the smoothness of the high repetition rate structure. The smooth appearance for the high frequency structure can be put in relation to a decrease in the material brittleness due to the unfinished dynamics.

From an application perspective, the radial extent of excitation makes the high energy pulse less desirable for transversal writing. We have therefore applied a higher energy pulse (1.1 μJ) for a longitudinal scan and we have obtained a smooth high refractive index structure [Fig. 9(a)] in contrast to the low-energy scan where the index variation is negative [Fig. 9(b)]. As mentioned, the transverse scan of the short pulse trace has produced a dominantly negative index variation [Fig. 9(c)]. In the OP case, the appearance of a positive index variation implies the possibility of obtaining a light-guiding structure by lateral scanning of this structure.

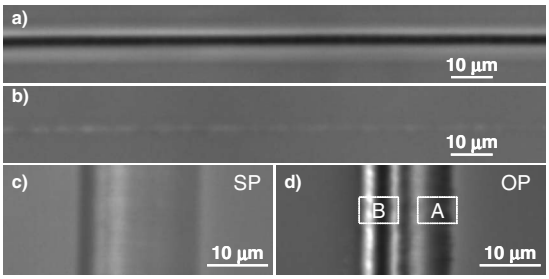

FIG. 9. (a) Short pulse longitudinal waveguides at high repetition rates (100 kHz). The energy per pulse was 1.1 μJ and the scan velocity was 50 μm/s. (b) Waveguide made by longitudinal writing using 0.25 μJ short pulses. (c) Transverse trace written by short laser pulses in the conditions of (a) at a scan velocity of 50 μm/s. (d) Transverse trace written by optimal laser pulses in the conditions of (a) at a scan velocity of 50 μm/s. Two regions of positive refractive index changes are indicated by the labels A and B.

The transversal scan of the optimal pulse trace at 1.1 μJ indicates the appearance of two main regions of high-contrast positive refractive index, which are labeled as A and B in Fig. 9(d). If zone A was already anticipated due to the material agglomeration at the tip of the exposed region, region B appears as a compression zone between two moving heat sources, which are already visible as structures in the optimal pulse trace.

V. CONCLUSION

In conclusion, we showed that extended regions of positive refractive index changes can be formed in optical materials with strong volume expansion. Premises for photoinscription of waveguiding structures are created at pulse repetition rates on the time scales of mechanical relaxation. Spatiotemporal design of ultrafast heat sources enforces key control factors for refractive index change: size, geometry, and temperature level of the heat source. A laser-triggered transition from radial thermal expansion to quasidirectional hydrodynamic flow was observed under optimal irradiation conditions, which is accompanied by refractive index flip. Creating positive refractive index changes in materials which do not allow it in standard irradiation conditions is beneficial for applications in the photonic technologies, enabling as well a fundamental perspective into the mechanisms of material changes on microscales.

ACKNOWLEDGMENTS

The financial support of GIP-ANR and PICS-2005 programs is gratefully acknowledged.

*Also at Department of Physics, Free University of Berlin.
†razvan.stoian@univ-st-etienne.fr

[1] K. Sokolowski-Tinten, J. Bialkowski, A. Cavalleri, D. von der Linde, A. Oparin and J. Meyerter-Vehn, and S. I. Anisimov, Phys. Rev. Lett. **81**, 224 (1998).
[2] S. Juodkazis, K. Nishimura, H. Misawa, T. Ebisui, R. Waki, S. Matsuo, and T. Okada, Adv. Mater. (Weinheim, Ger.) **18**, 1361 (2006).

[3] K. M. Davis, K. Miura, N. Sugimoto, and K. Hirao, Opt. Lett. **21**, 1729 (1996).
[4] V. R. Bhardwaj, E. Simova, P. B. Corkum, D. M. Rayner, C. Hnatovsky, R. S. Taylor, B. Schreder, M. Kluge, and J. Zimmer, J. Appl. Phys. **97**, 083102 (2005).
[5] D. Ehrt, T. Kittel, M. Will, S. Nolte, and A. Tünnermann, J. Non-Cryst. Solids **345-346**, 332 (2004).
[6] X. R. Zhang, X. Xu, and A. M. Rubenchik, Appl. Phys. A: Mater. Sci. Process. **79**, 945 (2004).
[7] S. Juodkazis, K. Nishimura, S. Tanaka, H. Misawa, E. G. Gamaly, B. Luther-Davies, L. Hallo, P. Nicolai, and V. T. Tikhonchuk, Phys. Rev. Lett. **96**, 166101 (2006).
[8] Y. Liu, H. Jiang, Q. Sun, Z. Wu, H. Yang, and Q. Gong, J. Opt. A, Pure Appl. Opt. **7**, 198 (2005).
[9] P. Martin, S. Guizard, Ph. Daguzan, G. Petite, P. D'Oliveira, P. Meynadier, and M. Perdrix, Phys. Rev. B **55**, 5799 (1997).
[10] J. W. Chan, T. R. Huser, S. H. Risbud, and D. M. Krol, Opt. Lett. **26**, 1726 (2001).
[11] A. Zoubir, M. Richardson, L. Canioni, A. Brocas, and L. Sarger, J. Opt. Soc. Am. B **22**, 2138 (2005).
[12] A. M. Streltsov and N. F. Borrelli, J. Opt. Soc. Am. B **19**, 2496 (2002).
[13] J. W. Chan, T. R. Huser, S. H. Risbud, J. S. Hayden, and D. M. Krol, Appl. Phys. Lett. **82**, 2371 (2003).
[14] K. Itoh, W. Watanabe, S. Nolte, and C. B. Schaffer, MRS Bull. **31**, 620 (2006).
[15] A. M. Weiner, Rev. Sci. Instrum. **71**, 1929 (2000).
[16] S. Nolte, M. Will, J. Burghoff, and A. Tünnermann, Appl. Phys. A: Mater. Sci. Process. **77**, 109 (2003).
[17] S. M. Eaton, H. Zhang, P. R. Herman, F. Yoshino, L. Shah, J. Bovatsek, and A. Y. Arai, Opt. Express **13**, 4708 2005.
[18] C. B. Schaffer, A. Brodeur, J. F. Garcia, and E. Mazur, Opt. Lett. **26**, 93 (2001).
[19] R. Osellame, N. Chiodo, V. Maselli, A. Yin, M. Zavelani-Rossi, G. Cerullo, P. Laporta, L. Aiello, S. De Nicola, P. Ferraro, A. Finizio, and G. Pierattini, Opt. Express **13**, 612 (2005).
[20] K. Miura, J. Qiu, H. Inouye, T. Mitsuyu, and K. Hirao, Appl. Phys. Lett. **71**, 3329 (1997).
[21] J. Burghoff, S. Nolte, and A. Tünnermann, Appl. Phys. A: Mater. Sci. Process. **89**, 127 (2007).
[22] C. Hnatovsky, R. S. Taylor, E. Simova, V. R. Bhardwaj, D. M. Rayner, and P. B. Corkum, J. Appl. Phys. **98**, 013517 (2005).
[23] C. Daniel, J. Full, L. Gonzalez, C. Lupulescu, J. Manz, A. Merli, Stefan Vajda, and L. Wöste, Science **299**, 536 (2003).
[24] A. Bartelt, Ph.D. thesis, Freie Universität Berlin, 2002.
[25] H. Zhang, S. M. Eaton, and P. R. Herman, Opt. Express **14**, 4826 (2006).
[26] I. Miyamoto, A. Horn, and J. Gottmann, J. Laser Micro/Nanoeng. **2**, 7 (2007).
[27] L. Sudrie, A. Couairon, M. Franco, B. Lamouroux, B. Prade, S. Tzortzakis, and A. Mysyrowicz, Phys. Rev. Lett. **89**, 186601 (2002).
[28] I. M. Burakov, N. M. Bulgakova, R. Stoian, A. Mermillod-Blondin, E. Audouard, A. Rosenfeld, A. Husakou, and I. V. Hertel, J. Appl. Phys. **101**, 043506 (2007).
[29] G. Cerullo, R. Osellame, S. Taccheo, M. Marangoni, D. Polli, R. Ramponi, P. Laporta, and S. De Silvestri, Opt. Lett. **27**, 1938 (2002).
[30] M. Lenzner, J. Krüger, S. Sartania, Z. Cheng, Ch. Spielmann, G. Mourou, W. Kautek, and F. Krausz, Phys. Rev. Lett. **80**, 4076 (1998).
[31] S. P. Timoshenko, *Course of Theory of Elasticity* (Naukova Dumka, Kiev, 1972) (in Russian).
[32] M. L. Wilkins, *Methods in Computational Physics* (Academic, New York, 1964), Vol. 3, p. 211.
[33] Y. P. Meshcheryakov and N. M. Bulgakova, Appl. Phys. A: Mater. Sci. Process. **82**, 363 (2006).
[34] M. Sakakura, M. Terazima, Y. Shimotsuma, K. Miura, and K. Hirao, Opt. Express **15**, 5674 (2007).
[35] A. Horn, E. W. Kreutz, and R. Poprawe, Appl. Phys. A: Mater. Sci. Process. **79**, 923 (2004).
[36] L. Hallo, A. Bourgeade, V. T. Tikhonchuk, C. Mezel, and J. Breil, Phys. Rev. B **76**, 024101 (2007).
[37] P. P. Rajeev, M. Gertsvolf, E. Simova, C. Hnatovsky, R. S. Taylor, V. R. Bhardwaj, D. M. Rayner, and P. B. Corkum, Phys. Rev. Lett. **97**, 253001 (2006).